JOURNAL OF AIRCRAFT
Vol. 47, No. 1, January–February 2010

Intelligent Flight-Trajectory Generation to Maximize Safe-Outcome Probability After a Distress Event

Nesrin Sarigul-Klijn,* R. Rapetti,† A. Jordan,‡ I. Lopez,† M. Sarigul-Klijn,§ and P. Nespeca†
University of California, Davis, Davis, California 95616

DOI: 10.2514/1.45264

A flight trajectory generation method called the distressed-aircraft-recovery technique for maximum safe-outcome probability (DART_MSOP), based on integration of three new algorithms, is developed that maximizes safe-outcome probability after a distress event by incorporating an abort airport together with a model of current aircraft dynamics. Several abort-probability models are studied under various constraints. The first new algorithm, a statistical-based initial-turn-determination algorithm, is developed to advise pilots to a reachable best landing site immediately after the distress event and before using the second new algorithm, a high-fidelity flight trajectory generation algorithm. A third new algorithm determines the flight maneuver for guidance of a perpetual-turning-attitude aircraft to fly the trajectory generated by the second algorithm. The third algorithm is only used if the aircraft has stuck controls or a similar malfunction that generates a nonzero amount of bank angle and causes the aircraft to turn only in one direction. As a three-dimensional high-fidelity algorithm, the second algorithm considers the probability of an abort to increase overall survivability by minimizing expected flight-path length as it shapes the trajectory. The performance of this new intelligent flight trajectory determination method DART_MSOP is evaluated using a case study based on a hypothetical in-flight distressed transport aircraft in northern California. Numerical simulations include variable failure rates to simulate different in-flight distress conditions, and multiple fixes along the path to accommodate realistic trajectories. DART_MSOP intelligent flight trajectory determination method should increase aviation safety if these algorithms are implemented in aircraft avionics systems.

Nomenclature

A	=	abort airport, airport A
B	=	better airport, airport B
b	=	wing span
C_L	=	lift coefficient
D	=	aircraft position at the distress event
$E(.)$	=	expected value
F_D	=	drag force
F_T	=	jet engine thrust
$g(s)$, $h(s)$	=	constraint function of inequality and equality
k, K	=	failure-rate shape parameter for Weibull probability distribution
m	=	aircraft total mass
$p(s)$	=	probability density function for an abort at a point along the path
R	=	radius of curvature along the trajectory
$r_{\min}$	=	aircraft minimum turn radius
s	=	curvilinear coordinate parameter along the flight path
W	=	aircraft total weight
x, y	=	Cartesian coordinates for the flight ground track
γ	=	flight-path angle
λ, μ	=	size parameter and mean value of the Weibull probability distribution
ρ	=	air density

Presented as Paper 2020 at the AIAA Infotech@Aerospace Conference, Seattle, WA, 6–9 April 2009; received 4 May 2009; revision received 5 October 2009; accepted for publication 5 October 2009.

*Professor, Mechanical and Aerospace Engineering Department; nsarigulklijn@ucdavis.edu. Associate Fellow AIAA (Corresponding Author).

†Ph.D. Candidate, Mechanical and Aerospace Engineering Department. Member AIAA.

‡M.S. Candidate, Mechanical and Aerospace Engineering Department. Member AIAA.

§Lecturer, Mechanical and Aerospace Engineering Department. Senior Member AIAA.

I. Introduction

IN-FLIGHT structural damage and actuator-fault-related control-surface failures are some of the causes of in-flight distress of transport-category aircraft [1,2]. The distressed-aircraft-recovery technique (DART) research team is working on flight trajectory generation research to maximize safe-outcome probability (MSOP) after occurrence of an in-flight distress condition. The trajectory-generation process continues to be a challenging research area and concerns all aircraft controlled by a pilot (human or autopilot) onboard system or by a no-pilot onboard system (remotely or autonomously controlled). Basic goals in trajectory generation are to increase safe operations of all aircraft under normal flight and to increase survivability of all aircraft following an in-flight distress event. The common practice after an in-flight distress event is to land at the nearest airport by changing the preplanned flight path without investigating other options. DART_MSOP is designed to investigate other possibilities to maximize safe-outcome probability of flight following a distress event.

Aircraft flight-path planning and trajectory-generation subjects have been investigated by many researchers during the past three decades. Reference [3] gives a comprehensive review of numerical flight-trajectory optimization algorithms. Recently, several investigators have studied aircraft trajectories under damage [4–10]. Reference [4] details an adaptive flight-planner approach as an online trajectory generator with variable autonomy. It is intended to enhance the flight management system with improved cockpit situational awareness. In [5] flight plans are defined as waypoints together with connecting segments using two-dimensional paths. Waypoints are added heuristically to eliminate steep flight-path angles in cases in which the landing site is very close or the aircraft is very high. Landing sites are selected after determination of the aircraft's reachable footprint and are ranked according to numerous features, including runway characteristics and current surface wind and weather conditions. The runways are prioritized after determining them to be feasible. In [6] a temporally dependent probabilistic

model is used for plan development. An expert specifies event probabilities and action delays allow for computation of state probabilities. State probabilities are used to choose goal paths and remove improbable states. A recent approach to the aircraft trajectory problem uses direct multiple shooting to give the optimal open-loop trajectory [8]. The trajectory is simulated via the inverse method. If the error between the trajectories is unacceptable, the optimization and inverse simulation parameters are adjusted. Otherwise, the trajectory is considered near-optimal. References [9,10] develop trajectories for unmanned vehicles under safety, time, and/or fuel-consumption constraints. Reference [11] details general optimization algorithms toolbox used for trajectory optimization.

Landing of a distressed aircraft after in-flight distress event has been a topic of interest in [1,2,4,5,12–18]. All deal with recovery of aircraft with control-surface (secondary structure) or hydraulic system failures, except the DART, which considers recovery of an aircraft with primary structural damage. DART integrates multiple disciplines and their interactions using high-fidelity and low-fidelity models. These areas are structures, aerodynamics, stability and control, propulsion, fluid–structure–thermal interactions (aeroelasticity, aerothermoservoelasticity), trajectory optimization, flight testing, and training of human pilot and/or autopilot to recover the aircraft from a distress event that includes structural damage [1].

The current paper details a new method added to DART in optimum trajectory shaping that meets the survivability requirements within the dynamic constraints of the distressed-aircraft limitations. In particular, we present a new flight trajectory generation method called the distressed-aircraft-recovery technique for maximum safe-outcome probability, based on integration of three new algorithms developed that maximizes safe-outcome probability after a distress event by incorporating an abort airport together with a model of current aircraft dynamics. Several abort-probability models are studied under various constraints. The approach developed increases overall survivability by minimizing the expected flight-path distance given the abort-probability model. The performance of the DART_MSOP method is evaluated using numerical simulations that include variable failure rates to simulate different in-flight distress conditions and using multiple fixes along the path to accommodate realistic trajectories.

II. Technical Challenges and Context Information

Flight-path planning and optimized-trajectory shaping for an aircraft in the presence of in-flight damage have many requirements. In the case of a damaged aircraft in which the preplanned flight path becomes untenable, the pilot has to recompute a path and fly to an alternate landing site, which the pilot must also find and evaluate in the midst of the emergency. The pilot must quickly evaluate aircraft damage, select a landing site, and generate a new flight path while flying a distressed aircraft. Decision-making in an already-high-stress environment is likely to produce errors and may cause accidents due to pilot overload.

The ultimate goal in trajectory generation is to achieve safe landing with zero casualties and no additional vehicle damage. This task faces a threefold challenge:

1) How can an uncertain scenario with unknown information and unpredictable human decisions be properly represented?

2) How can we decipher and make use of sensory data to preserve vehicle's health condition?

3) How can we integrate context information in stochastically optimal path planning?

One way of looking at the problem is to realize that simply landing the aircraft is not enough. The flight path is not really complete until all passengers and crew are off the aircraft and into a hospital, as needed. Hence, we define the following phases to a successful landing:

Phase 1 is en route flight and approach to landing. This phase encompasses the time from the distress event until the aircraft touches the runway. The primary contributor to further failure here is time in the air.

Phase 2 is touchdown/rollout. This phase covers from the time the aircraft touches the tarmac until it stops sliding or rolling. At this point, failure is a question of runway environment and approach velocity.

Phase 3 is evacuation/rescue. This phase covers from the time the aircraft stops and emergency situation is fully under control, such as verifying that all the injured passengers are in a hospital. The primary issue here is the airport's emergency resources, such as proximity of fire crews, ambulances and hospitals.

All the above phases are accounted for indirectly in the DART_MSOP, as detailed in the following sections. Our focus in this paper is primarily in the phase 1 portion of flight following a distress event.

III. Technical Approach and Derivation of Governing Equations

The first step following a distress event is to evaluate the maneuverability of the aircraft. An estimate is obtained based on energy height and excess power relations. If the aircraft can sustain flight, then we proceed with our new flight trajectory generation method called the DART_MSOP method, as depicted in Fig. 1.

DART_MSOP method integrates three new algorithms we developed and maximizes safe-outcome probability after a distress event by incorporating an abort airport together with a model of current aircraft dynamics. The first new algorithm, a statistical-based initial-turn-determination algorithm, is developed to advise pilots to a reachable best landing site immediately after the distress event and before using the second new algorithm, a high-fidelity flight trajectory generation algorithm. A third new algorithm determines the flight maneuver for guidance of a perpetual-turning-attitude aircraft to fly the trajectory generated by the second algorithm. The third algorithm is only used if the aircraft has stuck controls or a similar malfunction that causes a nonzero amount of bank angle and causes the aircraft to turn only in one direction.

Consider the hypothetical situation of an aircraft ground track depicted in Fig. 2. Airport A is a decommissioned military base, which has runways with desirable features, but has no fire crews. Further, it is far from any hospital. However, it is the closest to the damage-event site, but not by a drastic amount. Airport B is a fully functional international airport with full fire teams and a nearby trauma center, with plenty of ambulances onsite. Airport A is closest, but if a fire starts on landing or there are already injured passengers, there will not be anyone to put out the fire or to stabilize the injured.

In summary, we consider two outcomes: 1) a successful landing at airport B, the better airport, and 2) a successful abort to airport A, the abort airport.

A generic transport aircraft model is considered. Simulated distress-event numerical studies are based on in-flight sustained right-wing damage. Aircraft model parameters are adjusted to predict wing-damaged-aircraft characteristics. Dynamics of aircraft are described by differential equations of motions under a point-mass assumption and using flat-Earth inertial coordinates as reference:

$$\frac{\mathrm{d}x}{\mathrm{d}t} = V\cos(\psi)\cos(\gamma) \tag{1}$$

$$\frac{\mathrm{d}y}{\mathrm{d}t} = V\sin(\psi)\cos(\gamma) \tag{2}$$

$$\frac{\mathrm{d}h}{\mathrm{d}t} = V\sin(\gamma) \tag{3}$$

$$\frac{\mathrm{d}E}{\mathrm{d}t} = \frac{V(F_T - F_D)}{mg} \tag{4}$$

$$\frac{\mathrm{d}\psi}{\mathrm{d}t} = \frac{L\sin(\varphi)}{mV\cos(\gamma)} \tag{5}$$

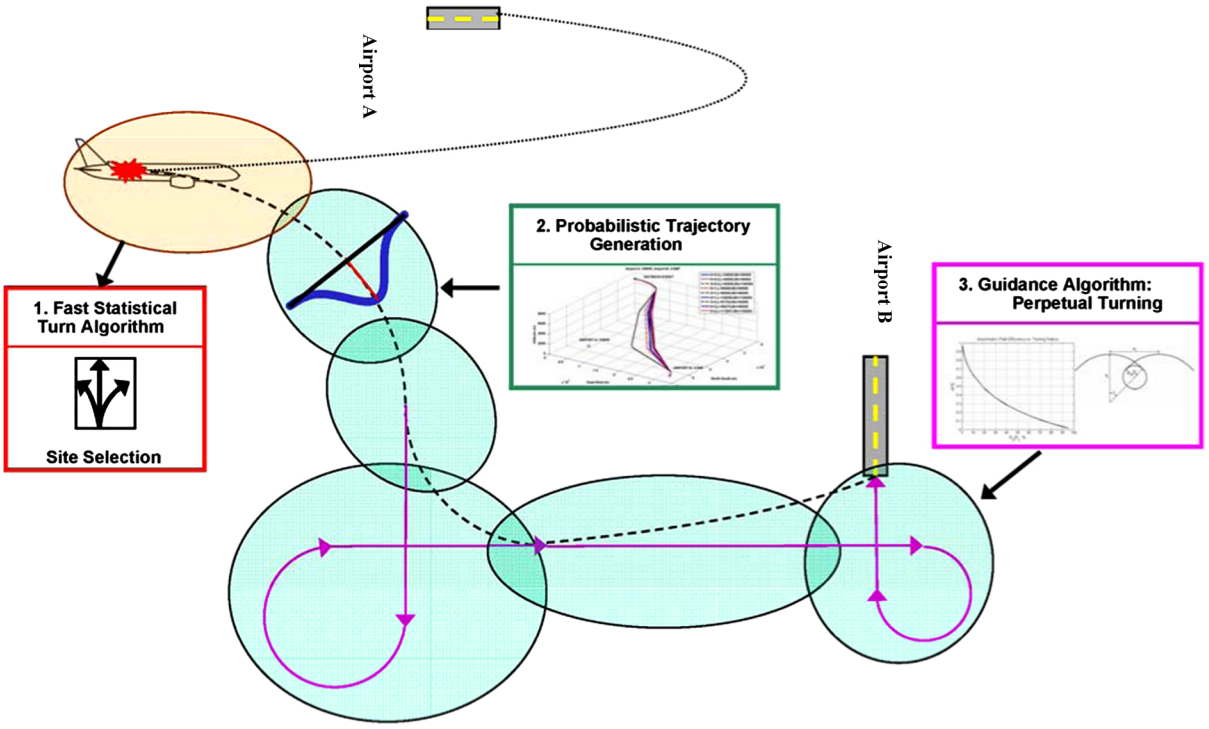

Fig. 1 DART_MSOP method with its three new algorithms for the abort and better airports, sketched for a perpetual-right-turning condition.

$$\frac{\mathrm{d}\gamma}{\mathrm{d}t} = \frac{L\cos(\varphi) - mgV\cos(\gamma)}{mV} \tag{6}$$

$$\frac{\mathrm{d}m}{\mathrm{d}t} = -c \tag{7}$$

where x and y are positions on flight ground track, h is altitude, H is energy height, ψ is heading angle, F_D is drag, T is thrust, V is velocity, g is gravitational acceleration, γ is flight-path angle, φ is bank angle, L is lift, c is constant fuel flow rate, and m is aircraft total mass. These equations can be decoupled for a constant-velocity flight. Other aircraft parameters that need to be considered following a damage event are load factor $n = L/g$ and wing loading W/S. In our DART_MSOP method, aircraft turn radius is used as a constraint in shaping the optimum trajectory using the following relation between the aerodynamics, flight loads, and aircraft current properties:

$$r_{\min} = \frac{2}{\rho g C_{L\max}}\left(\frac{W}{S}\right) \tag{8}$$

$$C_{L\max} = \frac{W}{1/2\rho V^2 S} \tag{9}$$

A more accurate evaluation of damaged-aircraft parameters can be obtained using formulations given in [2]. Equation (4) relates rate of change of energy height to specific excess power. It is used here to rapidly estimate maneuverability of aircraft before proceeding with flight-path generation using the DART_MSOP method.

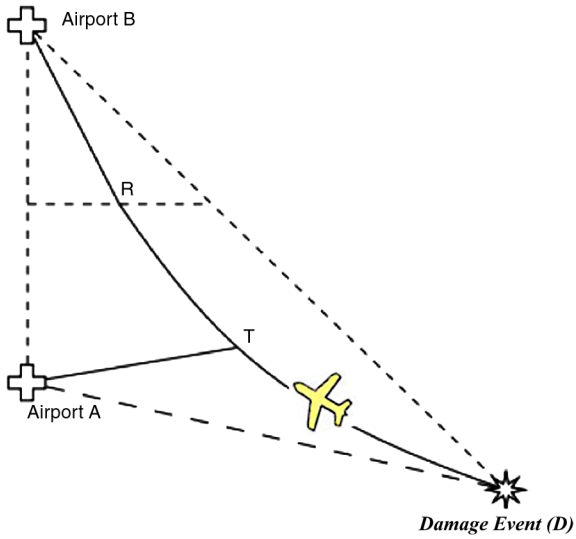

Fig. 2 Flight ground track, positions of D, A, B, T (the abort point along the path to B), and R (the point of no return along the path to airport B).

A. First New Algorithm of DART_MSOP: Statistical-Based Initial-Turn Determination

The first algorithm of the DART_MSOP method determines the initial turn toward the best landing sites using a statistical approach. This approach rank-orders best landing sites within seconds after a distress condition and assists pilots with the initial-turn decision toward the best airport and an abort airport before using the second new algorithm, a high-fidelity flight trajectory generation algorithm.

In some distress scenarios, one airport will stand out as the most probable option for success of the mission. In many other scenarios, the best option will stand out after statistical analysis of all relevant contextual information. This information is identified and related to aircraft, airport, and trajectory, as depicted in Fig. 3. Quantifiable factors are statistically analyzed in terms of three categories of deterministic, stochastic, and uncertain variables related to the maximization of safe-outcome probability. A mean value for each factor is established and compared with the specific value for each runway, resulting in a statistical score. Scores are totaled and displayed for the different airports. Statistical-based selection depends on the parameters included in Fig. 3.

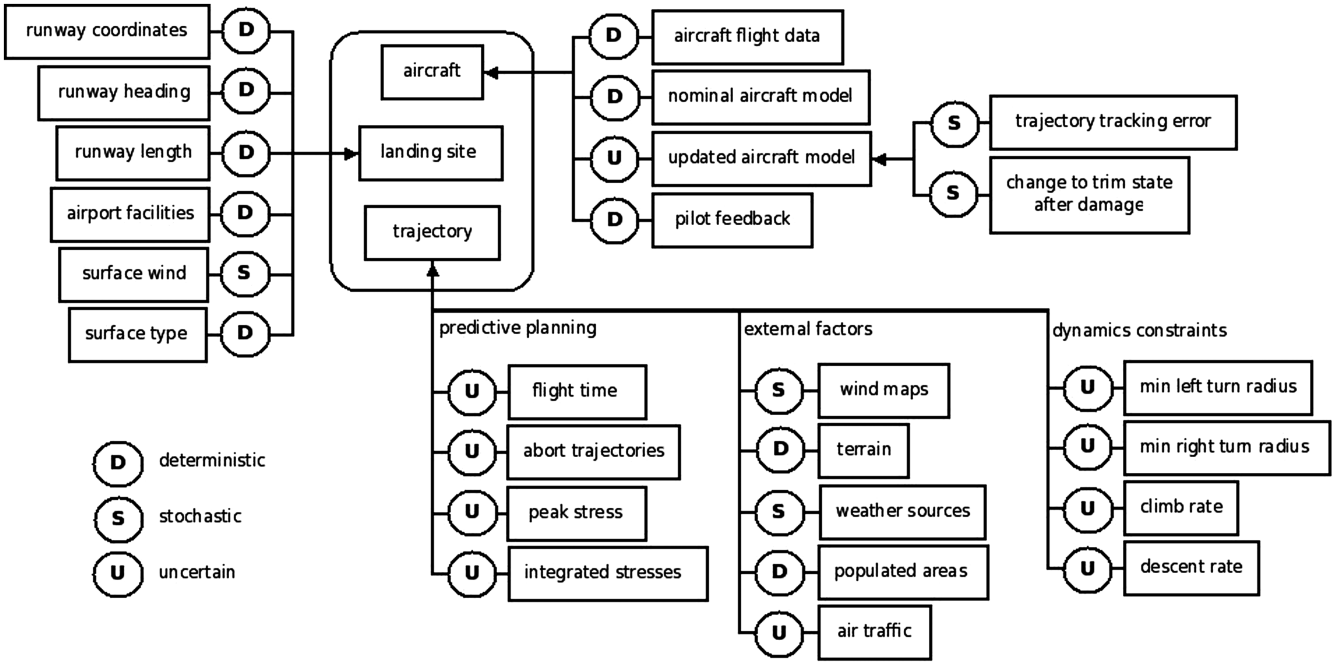

Fig. 3 Classification of quantifiable and imprecise variables related to a) distressed aircraft, b) landing site, and c) possible trajectory in three categories.

B. Second New Algorithm of DART_MSOP: Probabilistic-Based Flight-Trajectory Generation

As a three-dimensional high-fidelity algorithm, the second algorithm considers the probability of an abort to increase overall survivability by minimizing the expected flight-path length as it shapes the flight trajectory following the first algorithm. This high-fidelity probabilistic-based flight trajectory determination process consists of three main components:

1) The first component is the path representation. In our research we generated three-dimensional paths using path-following coordinates and fixes.

2) The second component is the probability model that accounts for the failure rates along the flight path after the distress event. This model represents the probable outcomes of a given path. In our research, the probability model is the probability density of each outcome as a function of position in space along the path.

3) The third component contains the objective-function formulation, its constraints, and the optimization algorithm. The objective function ties the outcomes together with their probabilities and the path into a measure of the usefulness of the path, which is then optimized under aircraft dynamic constraints to maximize the efficacy of the flight trajectory.

1. *Path Representation*

A path-following curvilinear coordinate s representation was developed to formulate three-dimensional aircraft paths. A path-following Cartesian unit vector set is also chosen, depicted in Fig. 4. $T_x(s)$ is the tangent vector along the trajectory and is positive from t to $t + \mathrm{d}t$ time, $T_y(s)$ is the normal to the trajectory along the radius of curvature and is positive toward the center of radius of curvature, and $T_z(s)$ is obtained from the vector product of x and y components.

This representation allows complex three-dimensional trajectories to be represented uniquely at each trajectory point. Aircraft body-fixed coordinates have the usual representation of the origin at aircraft center of gravity, tail to nose, and center of gravity to right-wingtip positive coordinates.

Two types of preshaped path segments are formulated. The first is from a fix to a fix. The second one is a base-to-final-leg segment.

A set of straight segments and constant-radius-of-curvature segments shown in Fig. 5 is used to formulate the path segment directly, to reduce computational time. The curved segments are in three-dimensional space and can be climbing or descending curved

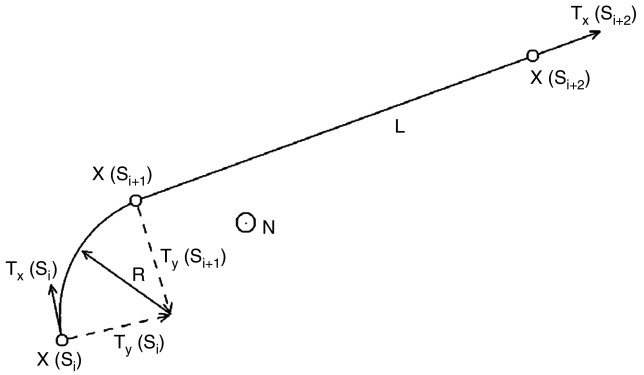

Fig. 5 Fix S_i to fix S_{i+2} transition schematic.

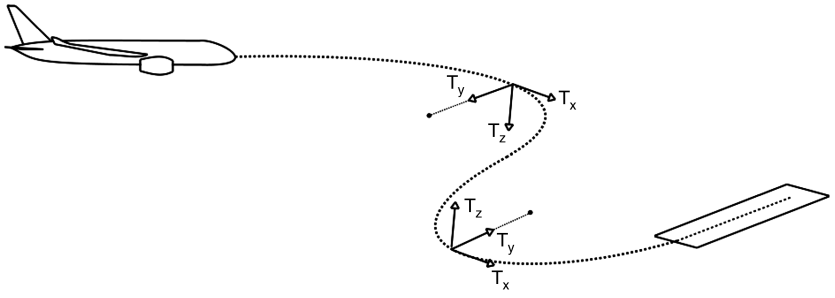

Fig. 4 Path-following curvilinear coordinates: T_x is tangent, T_y is along the radius of curvature, and T_z is perpendicular to the T_x–T_y plane.

segments. The method is vector-operation-based, which means that the intermediate form can be derived using linear algebra vector operations. One transformation in the three-dimensional case must be solved numerically. The positions at the starting point, starting orientation, and ending point are specified, and the ending orientation and curved-to-straight segment transition fix are determined.

The quantities $T_x(S_i)$, $X(S_i)$, and $X(S_{i+2})$, are known, and $T_x(S_{i+2})$, $X(S_{i+1})$, L, and N must be derived. The entire maneuver lies in the plane defined by the vectors $T_x(S_i)$, and $S_{i+2} - S_i$. N represents the vector normal to this plane:

$$N = \frac{T_x(S_i) \times (X(S_{i+2}) - X(S_i))}{\|T_x(S_i) \times (X(S_{i+2}) - X(S_i))\|} \tag{10}$$

All the values on the right side of this equation are known. The next step is to compute L. First, we must form a vector that points from $X(S_i)$ toward the center of curvature. This can be done by crossing $T_x(S_i)$ into N:

$$T_y(S_i) = T_x(S_i) \times N \tag{11}$$

Since these vectors are perpendicular unit vectors, no normalization is needed. Next, the center point of the curved segment can be computed:

$$C = X(S_i) + T_y(S_i)^* R \tag{12}$$

From geometry, we know that the distance from C to $X(S_{i+2})$ is

$$d = \|X(S_{i+2}) - C\| \tag{13}$$

From the Pythagorean theorem,

$$L = \sqrt{d^2 - R^2} \tag{14}$$

Now we must define a vector pointing from $X(S_{i+1})$ to C:

$$T_y(S_{i+1}) = T_x(S_{i+2}) \times N \tag{15}$$

and next, a vector traverse of the path,

$$X(S_i) + R^* T_y(S_i) - R^* T_y(S_{i+1}) + L^* T_x(S_{i+2}) = X(S_{i+2}) \tag{16}$$

Substituting Eq. (14),

$$-R^* T_x(S_{i+2}) \times N + L^* T_x(S_{i+2}) = X(S_{i+2}) - X(S_i) + R^* T_y(S_i) \tag{17}$$

Since the cross product can be expressed as a matrix multiplication, we can convert the vector N into the skew symmetric matrix N_m:

$$[L^* I + N_m] T_x(S_{i+2}) = X(S_{i+2}) - X(S_i) - R^* T_y(S_i) \tag{18}$$

Solving for $T_x(S_{i+2})$,

$$T_x(S_{i+2}) = [L^* I + N_m]^{-1} [X(S_{i+2}) - X(S_i) - R^* T_y(S_i)] \tag{19}$$

$X(S_{i+1})$ is derived as

$$X(S_{i+1}) = C - W^* R = X(S_{i+2}) - L^* T_x(S_{i+2}) \tag{20}$$

Equation (20) can be used to build the intermediate representation up to the final fix.

Figure 6 depicts the two-turn path segment used during landing. The problem has the additional constraint that the ending orientation must line up with the runway. Because of this, another degree of freedom is needed.

By adding a second turn, the path gains the flexibility necessary to match an ending orientation. There are two planes represented in the diagram: one defined by $X(S_i)$, $X(S_{i+1})$, and $X(S_{i+2})$ and another defined by $X(S_{i+1})$, $X(S_{i+2})$, and $X(S_{i+3})$. The governing equation for the three-dimensional case is presented as Eq. (21) and can be solved numerically:

$$X(S_i) + R^* T_y(S_i) - R^* T_y(S_{i+1}) + L^* V_{01} + R^* T_y(S_{i+2}) - R^* T_y(S_{i+3}) = X(S_{i+3}) \tag{21}$$

The vectors $T_y(S_i)$, $T_y(S_{i+1})$, $T_y(S_i + 2)$, and $T_y(S_{i+3})$ are computed similarly to the previous case. The difficulty arises in computing N_0 and N_1 normal directions. For the 3-D case, these are not readily computed, since the direction of the turn is always the same relative to the normal vector, and for the 2-D case, there is only one plane. One can easily see that there are four ways of arranging the vectors with the constraint that they must be normal to the plane: (out, out; out, in; in, out; in, in), which corresponds to the turn set $[R, R; R, L; L, R; L, L]$. Finding the optimal path is then a matter of computing all four combinations and choosing the shortest. The 3-D solution is found with a numerical optimization strategy. Equation (21) can be rearranged to equal zero when the solution is found, and hence the residual dotted with itself gives a least-squares objective function that can be driven to zero. The design variables in this case are the components of $T_x(S_{i+1})$, and the above equation can be manipulated to be a function of only these components, giving a three-variable optimization problem. The guess value for this optimization problem is computed by projecting the 3-D problem onto the plane defined by N_0 and $S_1 - S_0$. The 2-D problem can then be solved as described below, and the components of $T_x(S_{i+1})$ can be used as the initial conditions to solve the optimization problem.

The problem is solved by first projecting the 3-D problem onto the plane defined by $T_x(S_i)$ and $X(S_{i+3}) - X(S_i)$, forming two vectors, N and $T_x(S_{i+3})$, which are the plane normal vector and the normalized projection of $T_x(S_{i+3})$ onto the plane, respectively. As before, L is derived geometrically:

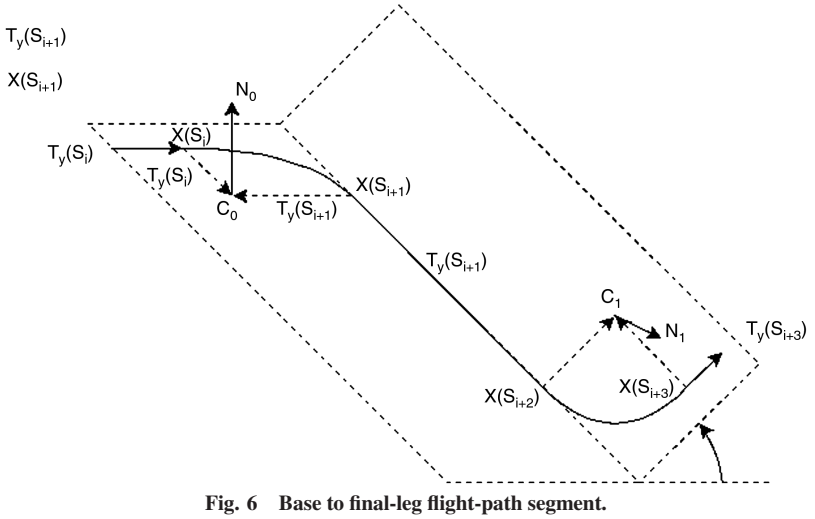

Fig. 6 Base to final-leg flight-path segment.

$$L = \sqrt{(C_1 - C_0)\cdot(C_1 - C_0) - (R^*N_1 - R^*N_0)\cdot(R^*N_1 - R^*N_0)} \tag{22}$$

The second set of terms under the radical takes care of the geometric differences between the cases: i.e., if the turns are the same direction (LL or RR), L is just the distance from turn center to turn center; otherwise, the Pythagorean theorem is used to find the diagonal. Next, since N_0 and N_1 are known, we can derive the four solutions based on

$$T_x(S_{i+1}) = T_x(S_{i+2}) = [L^*I + R^*N_{m0} - R^*N_{m1}]^{-1}[X(S_{i+3}) - X(S_i) - R^*T_y(S_i) + R^*T_y(S_{i+3})] \tag{23}$$

for the set

$$[N_0, N_1] = [N, N; N, -N; -N, N, -N, -N]$$

where N is the plane normal vector discussed above. From this family of solutions, the shortest (optimum) path can be chosen. The obtained value is then substituted into the residual equation:

$$r_e = X(S_i) - X(S_{i+3}) + R^*T_y(S_i) - R^*T_y(S_{i+1}) + L^*T_x(S_{i+1}) + R^*T_y(S_{i+2}) - R^*T_y(S_{i+3}) \tag{24}$$

The objective function J is optimized for the quantity $L^*T_x(S_{i+1})$:

$$J = r_e \cdot r_e \tag{25}$$

Note that since $T_x(S_{i+1})$ is a unit vector, only two of its components are independent. Adding L as a design variable brings the number of unknowns up to three. For transport-category aircraft, the planar guess will be very close to the real solution and the optimization will converge quickly, as shown during the case study conducted in this paper.

2. *Probability Density Function*

In this study we considered two types of probability density functions: namely, Weibull distribution and constant-valued functions, as detailed in the following section. To represent failure rates of distressed aircraft along the path, we chose the Weibull distribution because of its common use for failure prediction of engineering systems:

$$p(s) = \frac{k}{\lambda}\left(\frac{s}{\lambda}\right)^{k-1} e^{-(\frac{s}{\lambda})^k} \tag{26}$$

where λ is the position parameter of the distribution, which is proportional to the mean μ and related to the k shape parameter by the following equation:

$$\mu = \lambda \cdot \Gamma(1 + 1/k) \tag{27}$$

By analyzing real-world data when available, a better model could be derived to represent actual conditions. For now, we simulated different distressed conditions by varying the failure-rate parameter k as 1) k less than 1 to study decreasing failure rate, 2) $k = 1$ to study a constant failure rate, and 3) k larger than 1 to study an increasing failure rate.

Our DART_MSOP method is not tied in any way to a particular statistical model. The results are derived numerically; therefore, any statistical model can be used, as long as it obeys the usual rules governing probability density functions. For this case, only the distance along the path is used to calculate the probability of an abort. The results are derived numerically, so any statistical model can be used, as long as it obeys the usual rules governing probability density functions. In the following section we implement a constant-valued probability density function to see the effects of changing the distribution from constant Weibull.

In this section the abort-probability model is taken to be a constant-valued probability distribution, as depicted in Fig. 7. Under constant-valued probability density function and single-turn path formulation, we obtained an analytical expression for the expected path length. Analytical forms are useful in reducing prediction time under a distress condition. The closed-form solution of the expected path length becomes

$$E_P(x_T, y_T) = S_J(1 - P_a) + S_{JB} + \frac{P_a}{S_J}\left(\frac{1}{2}S_{DT}^2 + \frac{1}{2}S_{TJ}^2 + I_{DT} + I_{TJ}\right) \tag{28}$$

$$I_{DT} = \int_0^{S_{DT}} \sqrt{s^2 + L_{DA}^2 - 2sL_{DA}\cos\psi_{AT}}\,\mathrm{d}s \tag{29}$$

$$I_{TJ} = \int_0^{S_{TJ}} \sqrt{s^2 + L_{TA}^2 - 2sL_{TA}\cos\psi_{AJ}}\,\mathrm{d}s \tag{30}$$

where E_P is the expected path length; S_J is the distance from D to J along the path; S_{JB} is the distance from J to$B$ along the path; L_{DA} is the straight-line distance from D to A; ψ_{AT} is the angle created by points A, D, and T; ψ_{AJ} is the angle created by points A, T, and J.

Numerical results using constant-valued probability density function with Sacramento International as the better airport and Mather Federal as the abort airport showed that increasing the probability of abort P_a will move the path toward the abort airport. For the single-fix path generated, the path first moves toward the abort airport and then turns toward the better airport, as in Fig. 8a. The expected-path-length plot looks very flat along the path from the distress-event point to the better airport, as shown in a surface plot in Fig. 8b.

3. *Flight-Trajectory Optimization to Maximize Safe-Outcome Probability*

The optimization system consists of three components: the path, probability density function, and the objective function with its constraints. Given the abort-probability model from Sec. II and a path that will contain several segments, we can compute the expected length of the path from the probability of abort at any point along the nominal track. The optimal course of action is to simply go straight to airport B after reaching equidistance point R (Fig. 2). A mathematical way of looking at this is to say that the probability of an abort beyond this point is identically zero. The curvilinear coordinate of this point will be called S_R.

The definition of the expected value of a random variable is

$$E(X) = \int_X xf(x)\,\mathrm{d}x \tag{31}$$

where x is the value of the random variable, $f(x)$ is the probability of the random variable taking that value, and X is the region over which $f(x)$ is defined. For this to be valid, the following equation must be valid:

$$\int_X f(x)\,\mathrm{d}x = 1 \tag{32}$$

For this derivation, we will use a general probability density function $p(s)$. The expected path length becomes

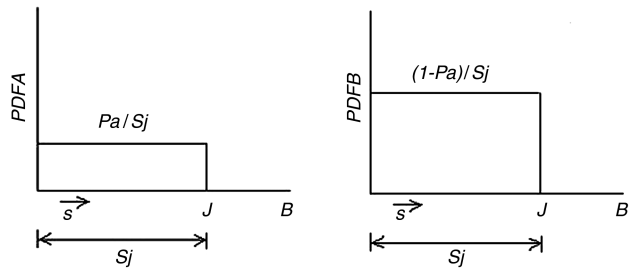

Fig. 7 Constant probability density function along flight-path ground track.

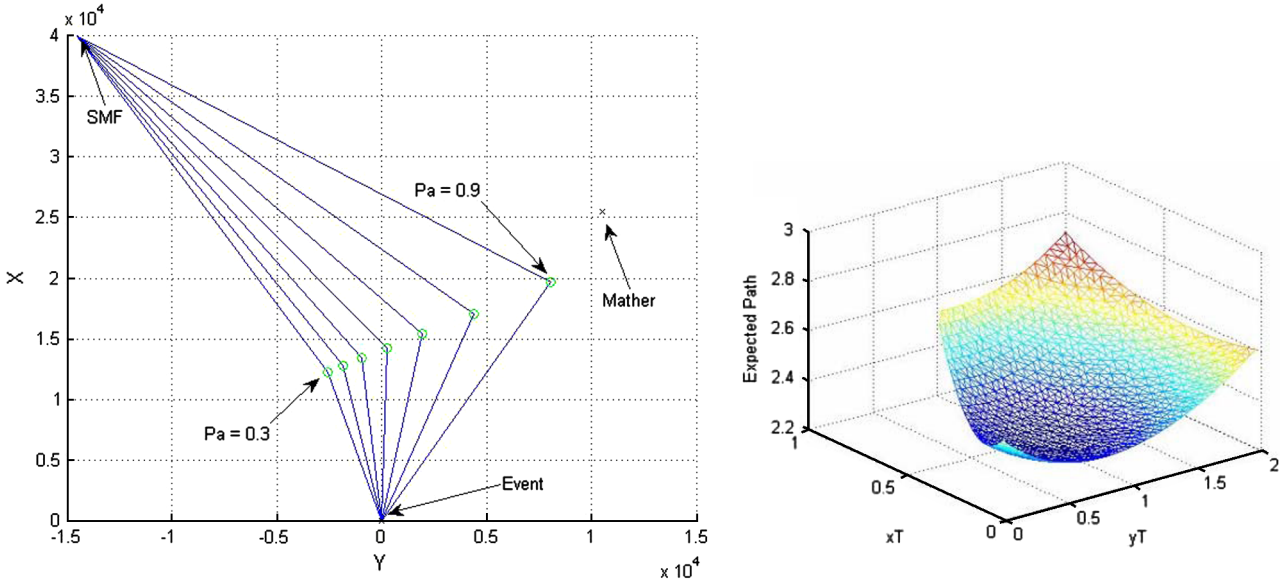

Fig. 8 Plots of a) effects of constant-valued probability density function on expected path length and b) expected path length's surface plot.

$$E_p = \int_0^{S_R} S_a(s)p(s)\,\mathrm{d}s + \int_{S_R}^{\infty} S_b p(s)\,\mathrm{d}s \tag{33}$$

There are two components to the integral because of the discrete nature of the probability model chosen. This arises because the path can take on a particular range from $s = 0, \ldots, S_R$ or a single discrete value of S_b, since the path length must take on this value for travel after S_R. So the first term takes care of the continuous range of the path length, and the second term accounts for the contribution of the single value. Taking advantage of the fact that

$$\int_0^{S_R} p(s)\,\mathrm{d}s + \int_{S_R}^{\infty} p(s)\,\mathrm{d}s = 1 \tag{34}$$

and that S_b is a constant, the above equation can be rearranged into the following:

$$E_p = \int_0^{S_R} S_a(s)p(s)\,\mathrm{d}s + S_b\left(1 - \int_0^{S_R} p(s)\,\mathrm{d}s\right) \tag{35}$$

The first term is continuous, and the second term is a single probability with a single value for the random variable. The expected path length can then be considered as the objective function. Finally, the expected distance can be minimized under the aircraft dynamic constraints through an optimization algorithm by using fixes, the minimum turn radius, and the flight-path angle constraints in shaping the turns. The constraints are included in a vector function forms of $g(s)$ and $h(s)$, and the optimization problem is stated as follows:

$$\text{Minimize } E_p = \int_0^{S_R} S_a(s)p(s)\,\mathrm{d}s + S_b\left(1 - \int_0^{S_R} p(s)\,\mathrm{d}s\right) \tag{36}$$

$$\text{Subject to } g(s) < 0 \quad \text{and} \quad h(s) = 0 \tag{37}$$

Using Lagrange multipliers Λ, the augmented functional for the optimization problem becomes

$$E_p^a = E_p + \Lambda_1 g(s) + \Lambda_2 h(s) \tag{38}$$

For the numerical case study presented in this paper, the constraints were

$$R(s) > R_{\min}(V, \rho, C_{l\max}, W/L) \tag{39}$$

and flight-path angles had limits of

$$-10 \le \gamma \le +10 \tag{40}$$

Optimization is required in many areas of the DART research; an optimization class was also developed that allows an optimizer to be integrated into any piece of software in a simple transparent manner. Each instance of the optimizer class is self-contained, so there is no concern about multiple optimizers interfering with one another. The optimization is conducted by writing an objective-function constraint function when applicable and setting the relevant parameters. The core of the optimization class is the Design Optimization Tools numerical optimization, [11]. This package is a set of FORTRAN tools for numerical optimization, both with and without constraints. Several algorithms are available, including MMFD, BFGS, Fletcher–Reeves CG, SLP, and SQP. In our DART_MSOP, the Fletcher–Reeves algorithm was used. The optimization is run on an Intel Core 2 quad-class desktop PC running Fedora Linux. Since the optimization is not multithreaded, it realizes no performance benefit from the extra cores. Even so, a single test case can be run in only 1–2 min, depending on the number of iterations required for a solution. Several changes could be made to significantly speed up the process. First, the algorithm computes the gradient of the objective function numerically, which requires many objective-function evaluations: on the order of 10–20 evaluations per iteration, depending on the number of fixes. Because of Moore's law, computational power should almost never be a limiting factor. If it runs in reasonable time on a basic desktop now, it is generally safe to assume that by the time the algorithm is implemented there will be more than sufficient computational power to run the algorithm in real time.

C. Third New Algorithm of DART_MSOP: Guidance Algorithm for Perpetual-Turning-Attitude Aircraft

A third new algorithm determines the flight maneuver for a perpetual-turning-attitude aircraft to fly the trajectory generated by the second algorithm [17]. In our DART_MSOP method the third algorithm is only used if the aircraft has stuck controls or a similar malfunction that generates a nonzero amount of bank angle and causes the aircraft to turn in only one direction. It may be noted that [18] gives a detailed mathematical proof for a similar condition without any practical reference.

A basic assumption is that it is not possible to trim the aircraft so that it is flying with its wings level. It is assumed that the aircraft can only make left or right turns exclusively. These assumptions are, in summary, as follows:

1) The aircraft can only be trimmed in a steady turn left or right turn, but not both.

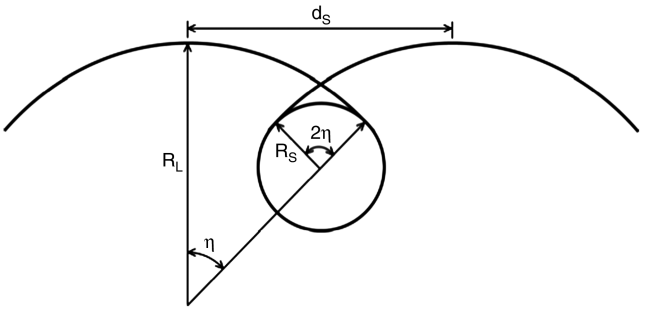

Fig. 9 The third new algorithm geometry parameters. The aircraft flies along a larger radius R_L until it sweeps a heading change of η (break angle), at which point the aircraft flies along a smaller radius R_S. The aircraft flies along the smaller radius for an arc that is $2\pi - 2\eta$. The straight-line distance traveled is d_s.

2) The aircraft can turn in two radii:R_L, a larger radius, and R_S, a smaller radius.

To achieve maximum range, the aircraft must fly as straight of a path as possible.

Figure 9 depicts the flight maneuver. It consists of alternating between the two radii separated by a break angle η. If one initially started out with a heading of 0 deg, one would fly the large radius R_L until the heading was η. Then one would fly the smaller radius until the heading was $-\eta$, at which point the larger radius would be flown again until the heading was η again. The only independent variable in this path is the break angle η. The idea is that there is an optimal break angle at which the path becomes most efficient. The asymmetric path efficiency (APE) is defined as

$$\text{APE} \equiv d_s/\text{total length traveled} \tag{41}$$

Using geometry, the APE can be obtained as

$$\text{APE} = (R_L - R_S)\sqrt{2(1-\cos(2\eta))}/(2R_L\eta + R_S(2\pi - 2\eta)) \tag{42}$$

Minimizing the 1-APE function gives the following results, shown in Figs. 10a and 10b. An analytical solution to the optimization was obtained by differentiating the APE expression with respect to η and setting that derivative to 0. This is expressed as

$$\tan(\eta) = \eta + \frac{\pi R_S}{(R_L - R_S)} \tag{43}$$

Equation (3) is a transcendental equation and cannot yield an exact analytical expression.

Figure 10b shows a reasonable trend: the efficiency starts at 1 and drops off quickly and eventually approaches zero value. Figure 10a shows a less-intuitive result, as the break angle increases sharply and tapers off. The break angle does seem to approach 90 deg for the degenerate case in which the two radii are identical.

These results are valuable in that they do not need to be implemented with an onboard computer. The pilot could perhaps have this data available in the form of a chart and make navigation decisions with this data. The path efficiency of Fig. 10b could help with range estimation, and the break-angle plot of Fig. 10a would dictate the path taken.

IV. Case Study: In-Flight Distressed-Aircraft Scenario in Northern California

A transport-category airplane encountered in-flight right-wing structural damage while on a descent out of flight level 200 (20,000 ft) into San Francisco International Airport (KSFO), as marked in sectional charts in Fig. 11. Indicated airspeed was 340 kt.

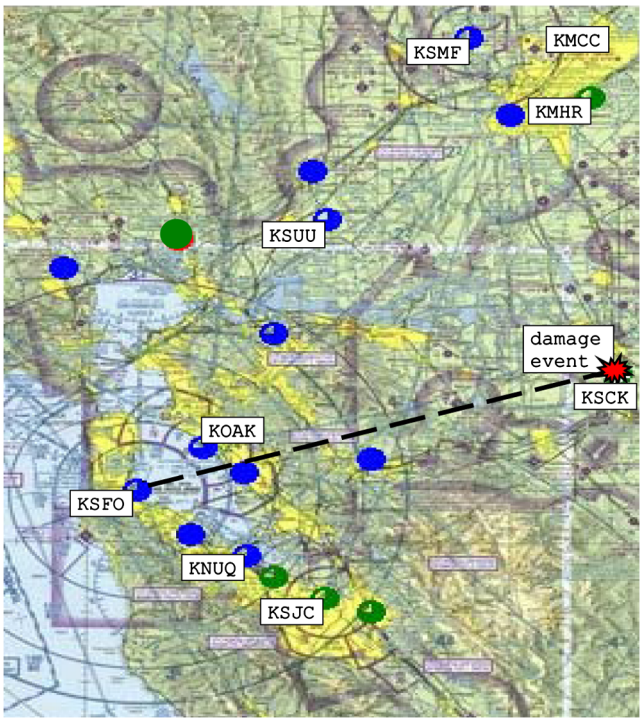

Fig. 11 Distress event and reachable airports. Note that for a regular approach, the airplane must reduce indicated airspeed to 250 kt below 10,000 ft.

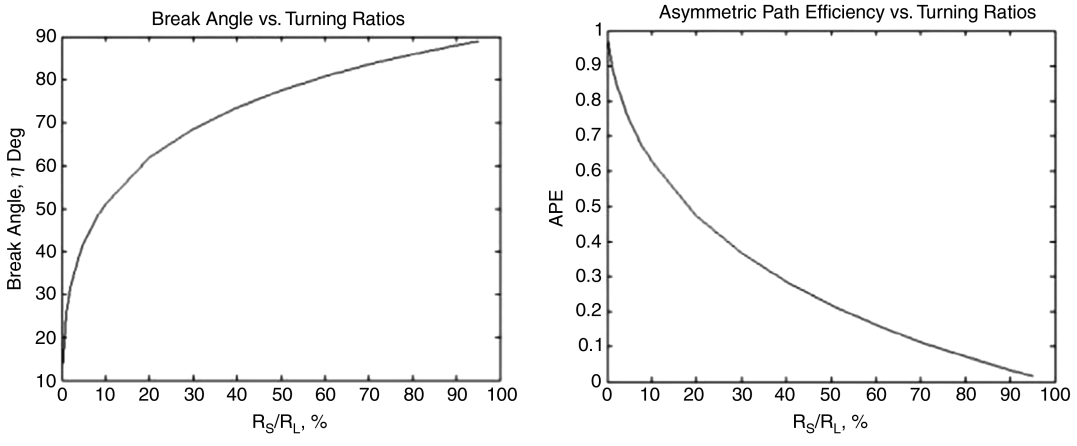

a) b)

Fig. 10 Plots of an optimum break angle η for a variety of turning ratios R_S/R_L and b) asymmetric path efficiency (APE) for a variety of turning ratios R_S/R_L.

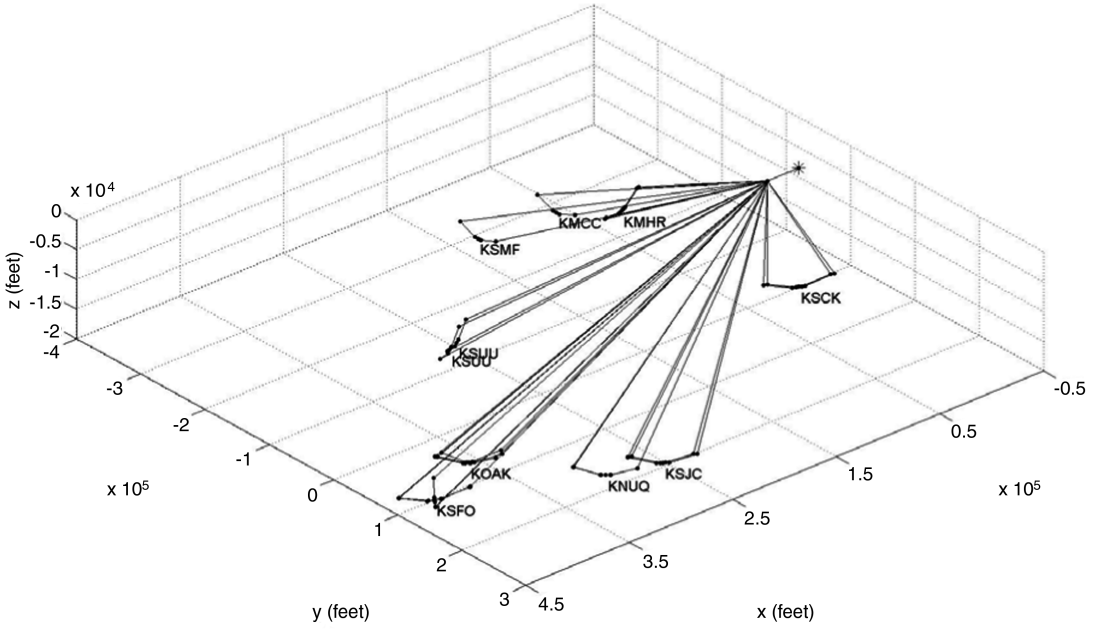

Fig. 12 Representation of scenario for statistical analysis.

The aircraft had departed New York with no problems; however, sudden changes occurred while passing North Stockton (KSCT). Based on the copilot's visual inspection, the damage was located on the outer-board wing. The pilots tried to maximize safe-outcome probability following this scenario. Possible airports and their identifiers are as follows: San Francisco (KSFO), Oakland (KOAK), San Jose (KSJC), Moffett Federal (KNUQ), Stockton (KSCK), Sacramento International (KSMF), Travis (KSUU), McClellan (KMCC), and Mather (KMHR).

Methods developed are applied for this scenario, first using a statistical approach for initial turn/landing sites rank-ordered. Then, using the highest-ranking three sets of runways, high-fidelity flight-optimized trajectories are generated using minimum turn radius as a constraint. For each destination and abort airport pair, nine cases are numerically simulated to represents various failure rates. This is accomplished by changing the parameters of the Weibull probability distribution function. A summary of the parameters varied for each destination and abort airport pair is provided in Table 1. The third algorithm was not needed to be executed for this case; results of the first and second algorithms are provided below.

A. Results from First New Algorithm of DART_MSOP: Statistical-Based Initial-Turn Determination

Consider three runway parameters: approach over a populated area, runway length, and approximate flight distance. Approach over a populated area takes a score of zero if true and one if false. The mean approximate flight distance score is obtained as the sum of the

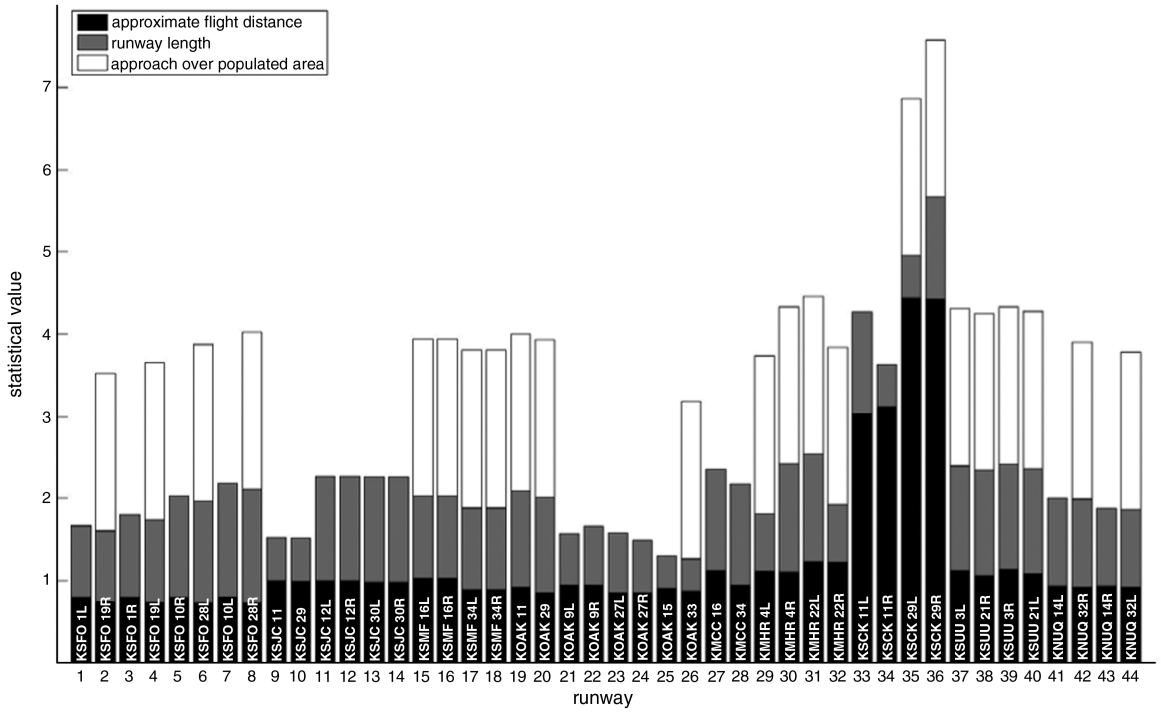

Fig. 13 Statistical analysis results shows the best landing sites to be Stockton, Mather Federal, and Travis.

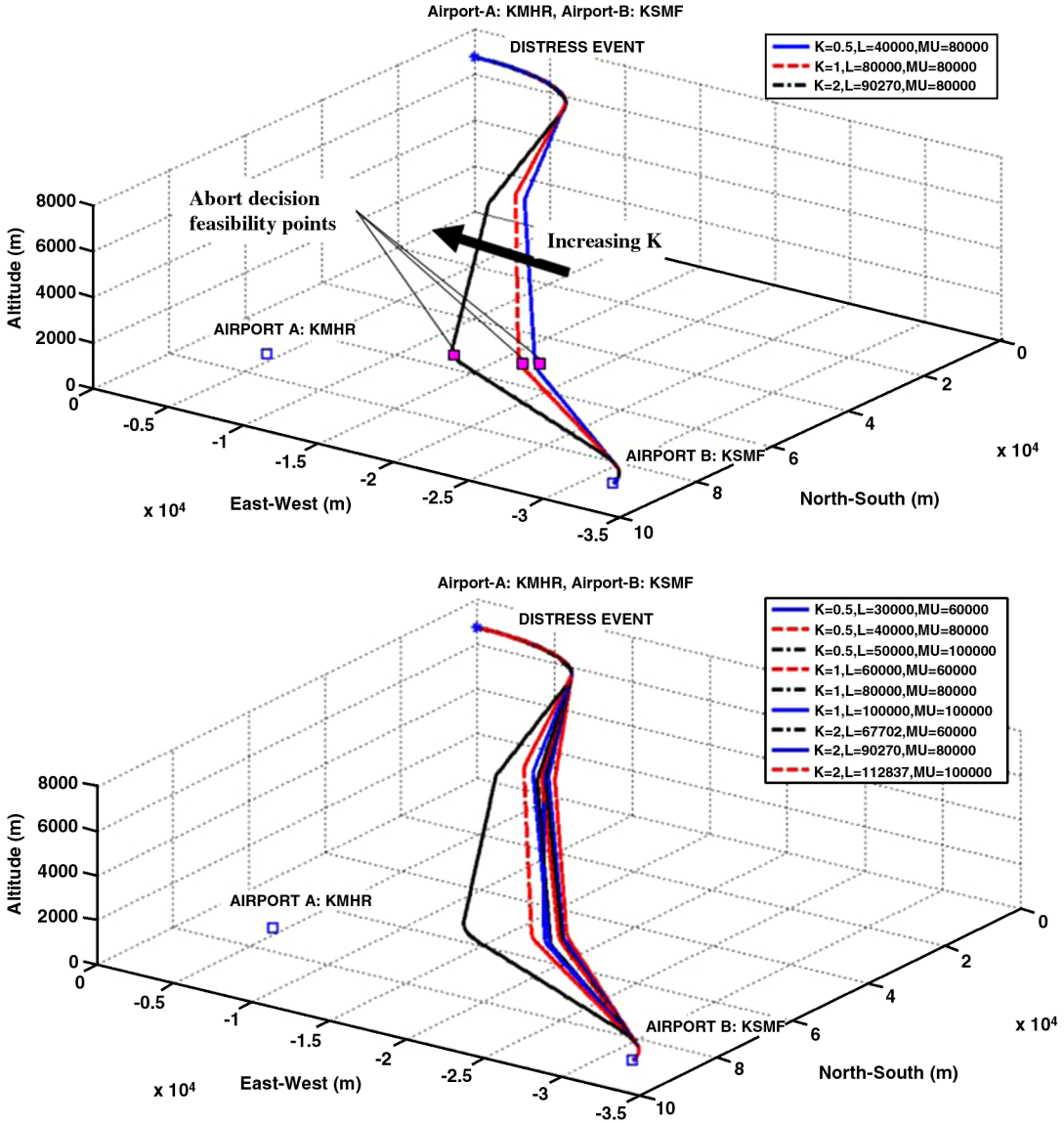

Fig. 14 Three-dimensional trajectory to Sacramento and Mather Federal for a) varying failure rates *K* and b) varying Weibull parameters.

approximate flight distances to all runways divided by the number of runways.

A statistical score for each runway is obtained by dividing the mean by the runway's approximate flight distance. Runway length and approach over a populated area scores differ in that the mean is the divisor. Once normalized by the mean values, the parameters are summed to represent an overall statistical score for each runway. The straight-line direct path, as shown in Fig. 12, used for approximate flight distance gives Stockton an advantage. The results in Fig. 13 show Stockton to be the best landing site. With the inclusion of additional, better-defined, parameters, this method can assist in landing-site selection.

B. Results from Second Algorithm of DART_MSOP: Three-Dimensional High-Fidelity Flight Trajectory

Several data items are extracted from each case study. First, the expected path length is studied. This is a measure of how effectively the path balances the conflicting objectives. Second, the overall probability of each outcome is also important. This is a good measure of how effective the path is at getting the aircraft to the desired airport. The average abort path length is also important, as it is a measure of how effective the method is at reducing abort path lengths compared with increases in nominal path length.

Parameter selection is critical to representing real-life flight scenarios and obtaining meaningful results. Data sets pertaining to the probability of an abort as a function of position are not available. For this research, best-estimate values are used.

There are two major parameters that must be chosen, both pertaining to the Weibull distribution. The first is λ, which is a measure of the location of the peak density of the probability distribution. The peak occurs at roughly λ. The exact solution has no closed form, but for reasonable parameter choices, the simplification is sufficient to make a guess at reasonable choices for λ. The second parameter is k, the failure rate. A value of $k < 1$ indicates a failure rate that decreases over time, whereas $k > 1$ indicates an increasing failure rate. The λ values are chosen based on the assumption that success when attempting to land at B is greater than 50%.

Figure 14 shows the effect of K on the shape of the optimal path. Since K is a failure-rate parameter, increasing K moves the probability density toward the end of the path. Since Mather Federal is close to the end of the nominal path for this case, increasing K pulls the end of the nominal path toward Mather Federal. Because that is the most likely area for an abort, being closer to Mather Federal at that point during the flight is advantageous if an abort should occur.

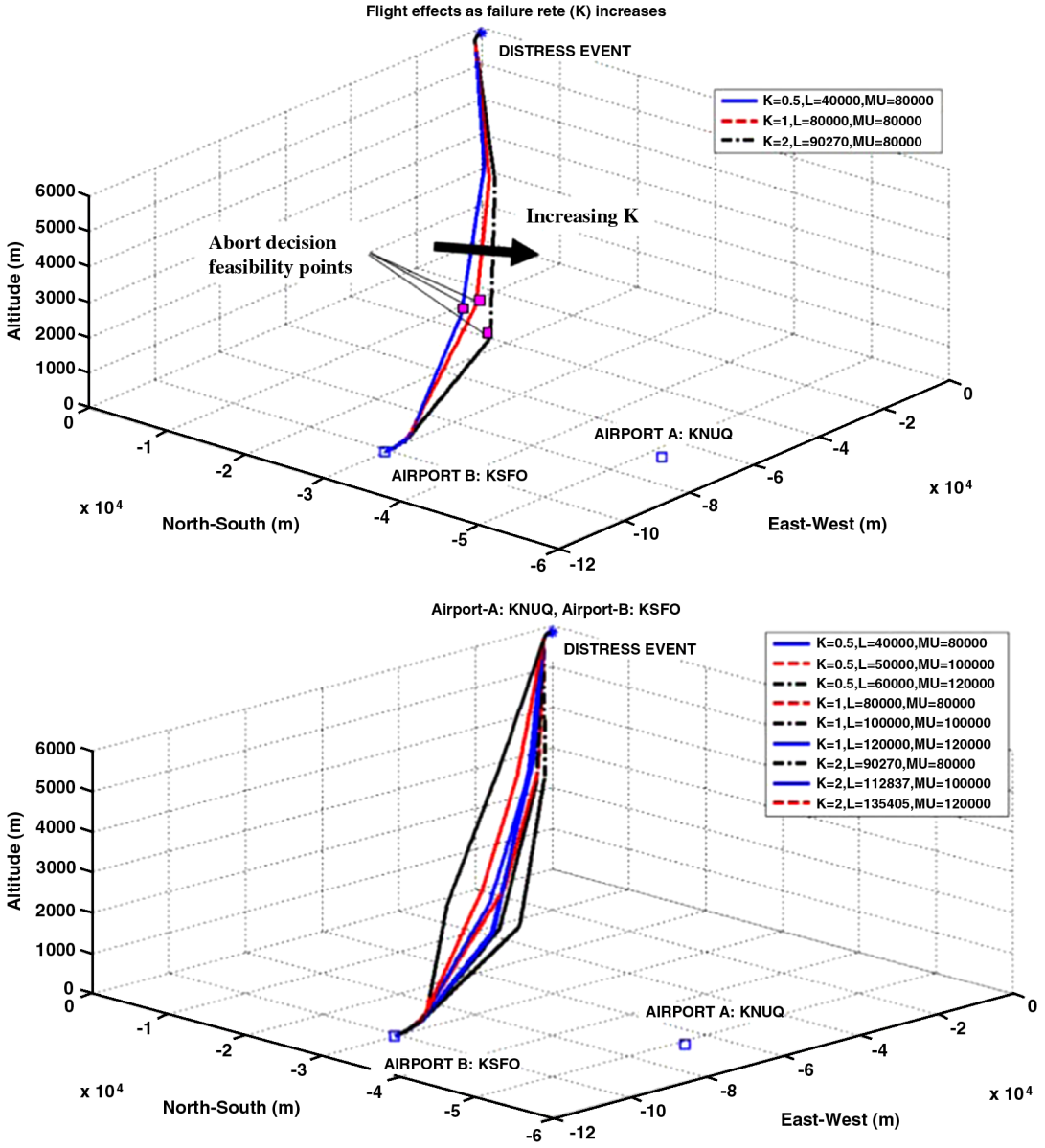

Fig. 15 Three-dimensional trajectory to San Francisco and Moffett for a) varying failure rates *K* and b) varying Weibull parameters.

For the other airport set in Fig. 15, similar behavior is observed. The behavior is not as pronounced, due to differences in the airport layout. Since Moffett Field is further away from the nominal path, getting closer has a higher cost than the KSMF/KMHR case; hence, the path does not pull in as close. The abort-feasibility decision points are the points along the path at which the distance to A and the distance to B are equal. This point is important because it is the last point at which an abort could be helpful, since from then on, the better airport will also be closer. The method shows the most bending behavior when K is large. This is not surprising, since the abort airport is near the end of the nominal path in both cases. Notably, the KSFO/KNUQ case showed the largest decrease in expected path length. This happened when $K = 2.0$ and $\lambda = 67,702$. Since the abort airport is further from the nominal path for this test case, optimization and the resultant bends in the path offer a larger advantage than when the abort airport is closer.

The complete data set is provided in Table 1.

V. Conclusions

The probabilistic-based flight-path architecture developed in this research offers marked improvement in the expected path length when the aircraft attempts to fly to a better airport. It also offers particular improvement in the path length if an abort does occur. This is important, as an abort will likely be accompanied by reduced range and/or maneuverability. Under a flight distress condition, distance to the landing site becomes even more important. Hence, the novel probabilistic method developed here offers improvement by reducing the expected path length while increasing the probability of safe landing, given the occurrence of an abort situation.

The maximum-range perpetual-turn flight-maneuver analytical method offers a way to handle the constrained nonzero-turn-rate problem in an optimal fashion. An expression for the most efficient entry and exit turn angles has been derived, allowing a pilot to maximize distance traveled while respecting turn-rate constraints of the damaged aircraft.

This research has several key innovations that will advance intelligent flight-path generation and contribute to flight safety. At present, the 3-D path optimization formulation is capable of optimizing paths to minimize expected path length. The architecture is modular and flexible to allow for more complex probability models and explicit consideration of an abort decision model. The performance of this new intelligent flight trajectory determination method is evaluated using a case study based on a hypothetical in-

Table 1 Parameters for each destination and abort airport pair

Nominal	Abort	K	λ	μ	Unoptimized			Optimized			Change after optimization		
					Expected path length	P_a, %	P_b, %	Expected path length	P_a, %	P_b, %	Expected path length, %	P_a, %	P_b, %
Scenario 1													
KSMF	KMHR	0.5	30,000	60,000	81,925.9	75.4	24.6	81,834.0	75.7	24.3	−0.11	0.29	−0.29
KSMF	KMHR	0.5	40,000	80,000	83,074.2	70.9	29.1	82,995.7	71.1	28.9	−0.09	0.22	−0.22
KSMF	KMHR	0.5	50,000	100,000	83,956.5	67.2	32.8	83,882.0	67.4	32.6	−0.09	0.19	−0.19
KSMF	KMHR	0.5	60,000	120,000	85,509.1	66.2	33.8	85,444.6	66.3	33.7	−0.08	0.13	−0.13
KSMF	KMHR	0.5	70,000	140,000	86,037.5	63.3	36.7	85,966.9	63.5	36.5	−0.08	0.13	−0.13
KSMF	KMHR	0.5	80,000	160,000	86,489.6	60.9	39.1	86,416.3	61.0	39.0	−0.08	0.13	−0.13
KSMF	KMHR	1.0	60,000	60,000	86,310.6	69.1	30.9	86,088.6	69.8	30.2	−0.26	0.76	−0.76
KSMF	KMHR	1.0	80,000	80,000	88,030.1	58.5	41.5	87,870.6	59.0	41.0	−0.18	0.49	−0.49
KSMF	KMHR	1.0	100,000	100,000	89,290.8	50.5	49.5	89,161.4	50.9	49.1	−0.14	0.31	−0.31
KSMF	KMHR	1.0	120,000	120,000	90,255.8	44.4	55.6	90,129.7	44.6	55.4	−0.14	0.22	−0.22
KSMF	KMHR	1.0	140,000	140,000	90,997.1	39.5	60.5	90,866.8	39.7	60.3	−0.14	0.15	−0.15
KSMF	KMHR	1.0	160,000	160,000	91,589.7	35.6	64.4	91,451.7	35.7	64.3	−0.15	0.13	−0.13
KSMF	KMHR	2.0	67,702	60,000	87,739.4	66.1	33.9	86,862.3	70.2	29.8	−1.00	4.08	−4.08
KSMF	KMHR	2.0	90,270	80,000	90,779.1	45.6	54.4	90,471.9	46.7	53.3	−0.34	1.09	−1.09
KSMF	KMHR	2.0	112,838	100,000	92,616.0	32.3	67.7	92,412.7	32.7	67.3	−0.22	0.42	−0.42
KSMF	KMHR	2.0	135,405	120,000	93,755.7	23.7	76.3	93,553.8	23.9	76.1	−0.22	0.18	−0.18
KSMF	KMHR	2.0	157,973	140,000	94,496.9	18.0	82.0	94,262.1	18.1	81.9	−0.25	0.04	−0.04
KSMF	KMHR	2.0	180,541	160,000	95,001.2	14.1	85.9	94,732.7	14.1	85.9	−0.28	−0.06	0.06
Scenario 2													
KSFO	KNUQ	0.5	30,000	60,000	94,095.7	75.5	24.5	93,462.9	76.9	23.1	−0.67	1.38	−1.38
KSFO	KNUQ	0.5	40,000	80,000	95,120.4	71.0	29.0	94,549.9	72.3	27.7	−0.60	1.28	−1.28
KSFO	KNUQ	0.5	50,000	100,000	95,891.1	67.3	32.7	95,364.7	68.5	31.5	−0.55	1.25	−1.25
KSFO	KNUQ	0.5	60,000	120,000	97,480.1	66.3	33.7	97,018.4	67.6	32.4	−0.47	1.32	−1.32
KSFO	KNUQ	0.5	70,000	140,000	97,910.6	63.4	36.6	97,910.2	63.3	36.7	0.00	−0.17	0.17
KSFO	KNUQ	0.5	80,000	160,000	98,276.1	61.0	39.0	98,275.7	60.8	39.2	0.00	−0.17	0.17
KSFO	KNUQ	1.0	60,000	60,000	98,818.1	69.3	30.7	97,757.6	73.1	26.9	−1.07	3.82	−3.82
KSFO	KNUQ	1.0	80,000	80,000	100,076.0	58.7	41.3	99,264.6	61.9	38.1	−0.81	3.11	−3.11
KSFO	KNUQ	1.0	100,000	100,000	100,981.0	50.8	49.2	100,315.0	53.5	46.5	−0.66	2.70	−2.70
KSFO	KNUQ	1.0	120,000	120,000	101,671.0	44.6	55.4	101,121.0	46.9	53.1	−0.54	2.25	−2.25
KSFO	KNUQ	1.0	140,000	140,000	102,192.0	39.7	60.3	101,728.0	41.7	58.3	−0.45	1.95	−1.95
KSFO	KNUQ	1.0	160,000	160,000	102,606.0	35.8	64.2	102,202.0	37.4	62.6	−0.39	1.63	−1.63
KSFO	KNUQ	2.0	67,702	60,000	100,310.0	66.6	33.4	97,988.6	76.7	23.3	−2.31	10.09	−10.09
KSFO	KNUQ	2.0	90,270	80,000	102,333.0	46.0	54.0	101,168.0	52.5	47.5	−1.14	6.44	−6.44
KSFO	KNUQ	2.0	112,838	100,000	103,525.0	32.6	67.4	102,872.0	36.3	63.7	−0.63	3.72	−3.72
KSFO	KNUQ	2.0	135,405	120,000	104,256.0	24.0	76.0	103,848.0	26.1	73.9	−0.39	2.16	−2.16
KSFO	KNUQ	2.0	157,973	140,000	104,728.0	18.2	81.8	104,430.0	19.8	80.2	−0.28	1.55	−1.55
KSFO	KNUQ	2.0	180,541	160,000	105,048.0	14.3	85.7	104,860.0	15.3	84.7	−0.18	1.06	−1.06

flight distressed transport aircraft in northern California. Numerical simulations include variable failure rates to simulate different in-flight distress conditions and include multiple fixes along the path to accommodate realistic trajectories. The DART_MSOP method should increase aviation safety if these algorithms are implemented in aircraft avionics systems.

Acknowledgments

This research was funded in part by the Integrated Resilient Aircraft Control project under NASA cooperative agreement NNX08AB96A. Grant Monitor was Nhan Nguyen.

References

[1] Sarigul-Klijn, N., Sarigul-Klijn, M., Rapetti, R., and Nespeca, P., "Distressed Aircraft Recovery Technique (DART)," *2007 Homeland Security Conference Proceedings*, PM&AM Research, Paper 2007: Sarigul-Klijn, 21–24 Aug. 2007.

[2] Sarigul-Klijn, N., Nespeca, P., Marchelli, T., and Sarigul-Klijn, M., "An Approach to Predict Flight Dynamics and Stability Derivatives of Distressed Aircraft," AIAA Atmospheric Flight Mechanics Conference, AIAA Paper 2008-6877, 2008.

[3] Betts, J., "Survey of Numerical Methods for Trajectory Optimization," *Journal of Guidance, Control, and Dynamics*, Vol. 21, No. 2, 1998, pp. 193–207. doi:10.2514/2.4231

[4] Atkins, E., "Dynamic Waypoint Generation Given Reduced Flight Performance," 42nd AIAA Aerospace Sciences Meeting and Exhibit, Reno, NV, Paper 2004-779, Jan. 2004.

[5] Atkins, E., Alonso, I., and Strube, M., "Emergency Flight Planning Applied to Total Loss of Thrust," *Journal of Aircraft*, Vol. 43, No. 4, 2006, pp. 1205–1216. doi:10.2514/1.18816

[6] Blackmore, L., "A Probabilistic Particle Control Approach to Optimal, Robust Predictive Control," AIAA Guidance, Navigation, and Control Conference and Exhibit, Keystone, CO, AIAA Paper 2006-6240, Aug. 2006.

[7] Jain, A. K., Duin, R. P. W., and Jianchang, M., "Statistical Pattern Recognition: A Review," *IEEE Transactions on Pattern Analysis and Machine Intelligence*, Vol. 22, No. 1, 2000, pp. 4–37. doi:10.1109/34.824819

[8] Karelahti, J., Virtanen, K., and Ostrom, J., "Automated Generation of Realistic Near-Optimal Aircraft Trajectories," *Journal of Guidance, Control, and Dynamics*, Vol. 31, No. 3, 2008, pp. 674–688. doi:10.2514/1.31159

[9] LaValle, S., *Planning Algorithms*, Cambridge Univ. Press, Cambridge, England, U.K., 2006.

[10] Sharma, R., "Locally Efficient Path Planning in an Uncertain, Dynamic Environment Using a Probabilistic Model," *IEEE Transactions on Robotics and Automation*, Vol. 8, No. 1, 1992, pp. 105–110. doi:10.1109/70.127244

[11] *DOT: Design Optimization Tools, User's Manual*, Vanderplaats Research & Development, Colorado Springs, CO, 2007.

[12] Kaneshige, J., and Gundy-Burlet, K., *Integrated Neural Flight and Propulsion Control System*, AIAA Paper 2001-4386.

[13] Burcham, F. W., Jr., Maine, T. A., Burken, J. J., and Bull, J., "Using Engine Thrust for Emergency Flight Control: MD-11 and B-747," NASA TM 1998-206552, 1998.

[14] Rapetti, R., Sarigul-Klijn, N., Jordan, A., Lopez, I., and Sarigul-Klijn, M., "A Novel Probabilistic Approach in Determination of Landing Site for Distressed Aircraft," *AIAA Meeting Papers on Disc* [CD-ROM], AIAA, Reston, VA, Aug. 2008.

[15] Sarigul-Klijn, N., Rapetti, R., Lopez, I., Jordan, A., Sarigul-Klijn, M., and Nespeca, P., "Dynamically Constrained Adaptive Flight Path Planning Using Predictive Algorithms," *NASA Aviation Safety Technical Conference* [CD-ROM], NASA, Oct. 2008.

[16] Sarigul-Klijn, N., Rapetti, R., Lopez, I., Jordan, A., Sarigul-Klijn, M., and Nespeca, P., "A Probabilistic Algorithm in Landing Site Selection of a Distressed Aircraft Including Effects of Failure Rates," ASME International, Paper IMECE 2008-68567, Boston, Nov. 2008.

[17] Sarigul-Klijn, N., Rapetti, R., Lopez, I., Jordan, A., Sarigul-Klijn, M., and Nespeca, P., "Intelligent Flight Trajectory Generation to Maximize Safe Outcome Probability After a Distress Event," AIAA Infotech@Aerospace Conference, AIAA Paper 2009-2020, Seattle, WA, Apr. 2009.

[18] Choi, H. J., and Atkins, E., "An Analytic Trajectory Planner for Aircraft with Severe Damage or Failures," AIAA Infotech@Aerospace Conference, AIAA Paper 2009- 2018, Seattle, WA, Apr. 2009.